Atmospheric
Chemistry
and Physics

Seasonal variation of aerosol iron solubility in coarse and fine particles at an inland city in northwestern China

Huanhuan Zhang[1,2], Rui Li[1], Chengpeng Huang[3], Xiaofei Li[4], Shuwei Dong[1], Fu Wang[3], Tingting Li[1], Yizhu Chen[1], Guohua Zhang[1], Yan Ren[3], Qingcai Chen[4], Ru-jin Huang[5], Siyu Chen[6], Tao Xue[7], Xinming Wang[1], and Mingjin Tang[1,2]

[1]State Key Laboratory of Organic Geochemistry, Guangdong Key Laboratory of Environmental Protection and Resources Utilization, Guangzhou Institute of Geochemistry, Chinese Academy of Sciences, Guangzhou, China
[2]College of Earth and Planetary Sciences, University of Chinese Academy of Sciences, Beijing, China
[3]Longhua Center for Disease Control and Prevention of Shenzhen, Shenzhen, China
[4]School of Environmental Science and Engineering, Shaanxi University of Science and Technology, Xi'an, China
[5]State Key Laboratory of Loess and Quaternary Geology, Institute of Earth Environment, Chinese Academy of Sciences, Xi'an, China
[6]College of Atmospheric Sciences, Lanzhou University, Lanzhou, China
[7]School of Public Health, Peking University, Beijing, China

Correspondence: Mingjin Tang (mingjintang@gig.ac.cn)

Abstract. This work investigated seasonal variation of aerosol iron (Fe) solubility for coarse ($> 1\,\mu m$) and fine ($< 1\,\mu m$) particles at Xi'an, a megacity in northwestern China impacted by anthropogenic emission and desert dust. Total Fe concentrations were lowest in summer and were similar in other seasons for coarse particles but lowest in summer and highest in spring for fine particles; for comparison, dissolved Fe concentrations were higher in fall and winter than spring and summer for coarse particles but highest in winter and lowest in spring and summer for fine particles. Desert-dust aerosol was always the major source of total Fe for both coarse and fine particles in all four seasons, but it may not be the dominant source of dissolved Fe. Fe solubility was lowest in spring for both coarse and fine particles and highest in winter for coarse particles and in fall for fine particles. In general, aerosol Fe solubility was found to be higher in air masses originating from local and nearby regions than those arriving from desert regions after long-distance transport. Compared to coarse particles, Fe solubility was similar for fine particles in spring but significantly higher in the other three seasons, and at a given aerosol pH range, Fe solubility was always higher in fine particles. Aerosol Fe solubility was well correlated with relative abundance of aerosol acidic species, implying aerosol Fe solubility enhancement by acid processing; moreover, such correlations were better for coarse particles than fine particles in all four seasons. Fe solubility was found to increase with relative humidity and acid acidity for both coarse and fine particles at Xi'an, underscoring the importance of aerosol liquid water and aerosol acidity in regulating Fe solubility via chemical processing.

1   Introduction

Deposition of aerosol particles is a major external source of dissolved iron (Fe) in many open oceans (Boyd and Ellwood, 2010; Tagliabue et al., 2017), significantly affecting primary productions in these regions (Moore et al., 2009; Tang et al., 2021) and thus the global carbon cycle (Martin, 1990; Jickells et al., 2005). Dissolved Fe has also been recognized as an important source of reactive oxygen species in aerosol particles via mechanisms such as the Fenton reaction (Zhang et al., 2008; Fang et al., 2017; Wang et al., 2022) and thus may have adverse impacts on human health (Kelly, 2003; Abbaspour et al., 2014). In addition, dissolved Fe could catalyze aqueous oxidation of SO_2 (Martin and Good, 1991; Alexander et al., 2009; Huang et al., 2014), leading to the formation of sulfate, a major secondary species in aerosol particles. The various impacts of aerosol Fe are largely determined by its fractional solubility (often abbreviated as solubility), which is the ratio of dissolved Fe to total Fe.

Due to the impacts of dissolved aerosol Fe on ocean biogeochemistry and human health, a number of studies have been conducted in the last 2–3 decades (Chen and Siefert, 2004; Baker and Jickells, 2006; Kumar et al., 2010; Sholkovitz et al., 2012; Mahowald et al., 2018; Meskhidze et al., 2019; Zhu et al., 2020; Baker et al., 2021; Ito et al., 2021), leading to significant advances in our knowledge of aerosol Fe solubility and sources of aerosol-dissolved Fe. For example, many studies (Baker and Jickells, 2006; Sholkovitz et al., 2012) observed the inverse relationship between Fe solubility and total aerosol Fe. It has been recently realized that non-desert-dust sources, such as anthropogenic emissions and biomass burning, can be important for dissolved aerosol Fe in many regions (Sholkovitz et al., 2009; Ito et al., 2019; Hamilton et al., 2020; Liu et al., 2022), though their contributions to total aerosol Fe are usually minor. Furthermore, atmospheric aging processes, such as acid processing and organic complexation, may substantially enhance the solubility of Fe in desert dust and coal fly ash (Paris et al., 2011; Shi et al., 2012; Chen and Grassian, 2013; Li et al., 2017).

Despite significant progress, it remains difficult for modeling studies to reproduce the wide range of Fe solubility observed for ambient aerosols (Mahowald et al., 2018; Meskhidze et al., 2019). The relative contribution of non-desert-dust sources, versus desert dust, to dissolved aerosol Fe is still rather uncertain (Myriokefalitakis et al., 2018; Ito et al., 2019). In addition, the impacts of chemical processing (especially organic complexation) on aerosol Fe solubility have yet to be quantified for ambient aerosols. Further field measurements are needed to reduce the uncertainties in aerosol Fe solubility in order to better understand the impacts of aerosol Fe on marine biogeochemistry and human health.

Sources, compositions and physicochemical properties are very different for coarse ($> 1\,\mu m$) and fine ($< 1\,\mu m$) particles (Seinfeld and Pandis, 2016). Therefore, aerosol Fe sol-

ubility may differ significantly and is regulated by different sources or processes for coarse and fine particles, as found by previous work (Sakata et al., 2022; Zhang et al., 2022). In addition, both sources and chemical processes of aerosol particles exhibit significant variability for different seasons, consequently leading to seasonal variations in aerosol Fe solubility. For example, desert-dust aerosol mainly occurs in spring at Xi'an, where our present work was conducted, while anthropogenic emission becomes more important in winter (Cao and Cui, 2021); furthermore, higher temperature in summer causes more ammonium to partition into the gas phase and thus leads to higher aerosol acidity (Ding et al., 2019; Zhou et al., 2022). As a result, examining the seasonal variability of aerosol Fe solubility may provide clues for and insights into factors which regulate Fe solubility. However, seasonal variation of Fe solubility has only been explored by a few previous studies (Chen and Siefert, 2004; Tao and Murphy, 2019; Yang et al., 2020; Yang and Weber, 2022). In the present work, we investigated seasonal variations of total Fe, dissolved Fe and Fe solubility for fine and coarse particles at Xi'an, a megacity in northwestern China severely affected by anthropogenic emission and desert dust (Cao and Cui, 2021).

2   Methodology

2.1   Sample collection

Aerosol sampling in Xi'an took place during 1–30 April 2021 (spring), 12 July to 14 August 2021 (summer), 7 October to 7 November 2021 (fall) and 26 November to 31 December 2020 (winter). Xi'an has a population of ~ 13 million and is located in the middle of the Guanzhong Plain, which is surrounded by the Qin Mountains and the Chinese Loess Plateau (Fig. S1 in the Supplement), favoring accumulation of air pollutants and formation of severe air pollution (Cao and Cui, 2021). In addition, Xi'an is adjacent to major deserts in China and is thus frequently affected by desert-dust aerosol.

Sampling in winter took place at an urban site (34.23° N, 108.89° E), which is close to a busy major road and is located in residential and commercial areas (Cao et al., 2012), and was carried out on a building roof ($\sim 10\,m$ from the ground) at the Institute of the Earth's Environment, Chinese Academy of Sciences. Sampling in the other three seasons took place at another urban site (34.37° N, 108.97° E), which is located in residential areas (Chen et al., 2021), and was carried out on a building roof ($\sim 40\,m$ from the ground) at Shaanxi University of Science and Technology. Meteorological parameters (wind speed and direction, temperature and relative humidity) and $PM_{2.5}$ and PM_{10} mass concentrations were provided by nearby environmental monitoring stations.

Coarse ($> 1\,\mu m$) and fine ($< 1\,\mu m$) aerosol particles were collected onto Whatman 41 (W41) cellulose filters on a daily basis (from 08:00 to 07:30 the next day) using a two-stage aerosol sampler (TH-150C, Tianhong Co., Wuhan, China)

with a flow rate of $100 \, \mathrm{L} \, \mathrm{min}^{-1}$. W41 filters, which were used for aerosol sampling, were acid-washed to reduce background levels. After aerosol collection, filters were sealed individually in clean plastic Petri dishes and then stored at $-20\,^\circ\mathrm{C}$ for further analysis. Our previous work (Zhang et al., 2022) described filter pretreatment, aerosol sampling and filter storage in detail. In the present work, 28, 32, 30 and 36 pairs of filter samples were collected in spring, summer, fall and winter, respectively.

In our work, mass concentrations of various species in air, including $PM_{2.5}$ and PM_{10} concentrations, are reported under standard state conditions (at $0\,^\circ\mathrm{C}$ and 1 atm) to remove the effects of variations in temperature and atmospheric pressure.

2.2 Sample processing and analysis

Sample analysis was detailed in our previous work (Zhang et al., 2022; Li et al., 2023), and as a result, here we only provide key information in brief. Every filter was equally halved. The first half-filter, which was used to determine total Fe, was digested in a Teflon jar using microwave digestion; after residual acids used in digestion were evaporated, the Teflon jar was cooled to room temperature and then filled with $20 \, \mathrm{mL} \, HNO_3$ (1 %). The solution was filtered using a polytetrafluoroethylene (PTFE) membrane syringe filter (pore size: $0.22 \, \mathrm{\mu m}$) and then analyzed using inductively coupled plasma mass spectrometry (iCAP Q, Thermo Fisher Scientific, USA). In total, 14 elements were determined, including Fe, Al and Pb, and the recovery rates were found to be 90 %–110 % for Fe using certificated reference materials (GBW07454 and GSB07-3272-2015).

The other half-filter, which was used to determine dissolved Fe and soluble ions, was immersed in $20 \, \mathrm{mL}$ ultrapure water for 2 h, during which an orbital shaker ($300 \, \mathrm{r} \, \mathrm{min}^{-1}$) was used to stir the aqueous mixture. After that, the aqueous mixture was filtered using a PTFE membrane syringe filter (pore size: $0.22 \, \mathrm{\mu m}$) and then divided further into two parts. The first solution ($\sim 10 \, \mathrm{mL}$) was analyzed by ion chromatography to measure soluble anions and cations; the second solution ($10 \, \mathrm{mL}$) was acidified to contain 1 % HNO_3 (using $147 \, \mathrm{\mu L} \, 67 \% \, HNO_3$) and subsequently analyzed using inductively coupled plasma mass spectrometry.

2.3 Aerosol acidity calculation

The ISORROPIA-II model (Fountoukis and Nenes, 2007) was used in the "metastable + forward" mode to calculate aerosol pH for coarse and fine particles, and input data included concentrations of soluble anions (SO_4^{2-}, NO_3^- and Cl^-) and cations (NH_4^+, Na^+, K^+, Ca^{2+} and Mg^{2+}), temperature and relative humidity (RH). The effects of $NH_3(g)$ and $HNO_3(g)$ were not taken into account as their concentrations were not measured; this may cause some biases (likely underestimation) in calculated aerosol pH (Guo et al., 2015;

Hennigan et al., 2015; Pye et al., 2020), but the overall trend of aerosol pH would not be significantly affected. The reverse mode was not used in our work, as results calculated using the reverse mode are very sensitive to uncertainties in concentrations of common aerosol ions (Hennigan et al., 2015). Coarse particles are generally expected to be less acidic than fine particles, and it is not clear yet why similar and even lower aerosol pH was observed for coarse particles (when compared to fine particles) in spring and fall at Xi'an (Fig. S14). This may be caused by biases in aerosol pH calculation, and lower aerosol pH values were also reported in previous work for coarser particles carried out in northern Colorado, United States (Young et al., 2013). Concurrent measurements of gaseous NH_3, HNO_3 and HCl would help reduce uncertainties in calculated aerosol pH and have been implemented in our following studies since July 2022.

2.4 Air mass back-trajectory analysis

The HYSPLIT (Hybrid Single-Particle Lagrangian Integrated Trajectory)-4 model (Draxier and Hess, 1998) was employed to calculate 48 h air mass back trajectories using meteorological data (horizontal resolution: $1^\circ \times 1^\circ$; time resolution: 3 h) from the Global Data Assimilation System provided by the National Centers for Environmental Prediction. Back trajectories were determined with an arrival height of 100 m a.g.l. and arrival times of 08:00, 14:00, 20:00 and 02:00 on the next day (Wang et al., 2020), and every day four back trajectories were obtained. In total, 120, 136, 128 and 144 back trajectories were obtained in our work for spring, summer, fall and winter, and all the back trajectories were clustered using the cluster analysis method described elsewhere (Baker, 2010).

3 Total and dissolved aerosol Fe

3.1 Meteorological conditions and aerosol concentrations

The climate in Xi'an (and the Guangzhou Plain in general) is mainly regulated by the East Asian monsoon. During our campaign, the prevailing wind directions were west and southwest in spring, northeast in summer, southwest and northeast in fall, and west in winter (Fig. S2); furthermore, average wind speeds were $> 2 \, \mathrm{m} \, \mathrm{s}^{-1}$ in summer and fall and $< 2 \, \mathrm{m} \, \mathrm{s}^{-1}$ in spring and winter. Median temperatures were 13.6, 27.0, 12.7 and $1.3\,^\circ\mathrm{C}$ in spring, summer, fall and winter, and median RH was found to be 85 %, 71 %, 83 % and 77 % (Table S1 in the Supplement). Precipitation mainly took place in summer during our campaign in 2021, similarly to previous years (Cao and Cui, 2021).

Table S2 shows $PM_{2.5}$ and PM_{10} concentrations at Xi'an in the four seasons. PM_{10} concentrations were in the ranges of 15–243, 24–76, 22–151 and $41–212 \, \mathrm{\mu g} \, \mathrm{m}^{-3}$ in spring, summer, fall and winter, and the average values were
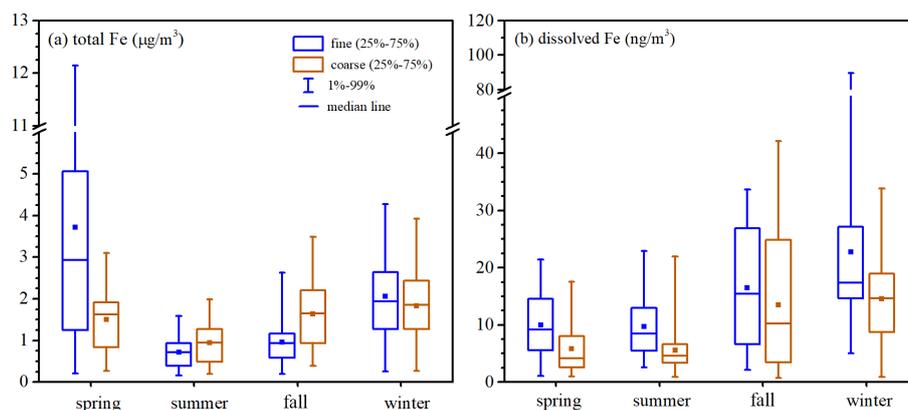
Figure 1. Seasonal variations of **(a)** total Fe and **(b)** dissolved Fe for fine and coarse particles.

93 ± 61, 51 ± 16, 70 ± 35 and $107 \pm 39 \, \mu g \, m^{-3}$, suggesting the highest levels in spring and winter and the lowest levels in summer. $PM_{2.5}$ mass concentrations were in the ranges of 11–62, 11–48, 13–97 and 13–$156 \, \mu g \, m^{-3}$, and the average values were 35 ± 14, 23 ± 8, 40 ± 24 and $80 \pm 32 \, \mu g \, m^{-3}$, suggesting the highest concentrations in winter and the lowest levels in summer.

$PM_{2.5}$ and PM_{10} concentrations were high in winter due to accumulation of anthropogenic pollution, and the median $PM_{2.5} / PM_{10}$ ratio was 0.76. PM_{10} concentrations in spring were significantly increased due to the impacts of desert-dust aerosol, and the median $PM_{2.5} / PM_{10}$ ratio was only 0.44. Two major dust events occurred during our spring campaign (12–17 and 27–30 April). During the two dust events the average PM_{10} and $PM_{2.5}$ mass concentrations were 151 ± 57 and $42 \pm 12 \, \mu g \, m^{-3}$, and $PM_{2.5} / PM_{10}$ ratios became even lower (0.20–0.31). Furthermore, the median $PM_{2.5} / PM_{10}$ ratios were 0.44 in summer and 0.62 in fall.

3.2 Total aerosol Fe

Figure 1a shows the seasonal variation of total aerosol Fe in coarse and fine particles measured by our work at Xi'an. Total aerosol Fe concentrations were in the ranges of 270–3095, 191–1992, 395–3492 and 269–$3924 \, ng \, m^{-3}$ for coarse particles in spring, summer, fall and winter, and the average values were 1504 ± 800, 950 ± 524, 1638 ± 830 and $1831 \pm 866 \, ng \, m^{-3}$ (Table A1 in the Appendix); total aerosol Fe concentrations were in the ranges of 206–12 144, 164–1591, 196–2631 and 257–$4268 \, ng \, m^{-3}$ for fine particles in spring, summer, fall and winter, and the average values were 3717 ± 3387, 721 ± 366, 958 ± 516 and $2058 \pm 1037 \, ng \, m^{-3}$. Average total Fe concentrations were measured to be 798 ± 466 and $801 \pm 534 \, ng \, m^{-3}$ for coarse and fine particles in winter (November–December 2019) at Qingdao (Zhang et al., 2022), only 44 % and 38 % of the average values (1831 ± 866 and $2058 \pm 1037 \, ng \, m^{-3}$) found in winter (November–December 2020) at Xi'an by the present

work, mainly because during wintertime aerosol mass concentrations were much higher at Xi'an than Qingdao.

The average contributions of coarse particles to total Fe in TSPs (total suspended particles) were 29 %, 57 %, 63 % and 47 % in spring, summer, fall and winter, being lowest in spring, when the influence of desert-dust aerosol was largest. Statistical analysis (paired t test) suggested that, compared to fine particles, total Fe in coarse particles was significantly lower in spring ($p < 0.01$, $\alpha = 0.05$) but significantly higher in summer and fall ($p < 0.01$, $\alpha = 0.05$); in addition, there was no significant difference between coarse and fine particles in winter ($p = 0.13$, $\alpha = 0.05$). The average contributions of coarse particles to total Al in TSPs were 26 %, 50 %, 54 % and 40 % in spring, summer, fall and winter, also being lowest in spring. Furthermore, during dust periods (12–17 and 27–30 April), the average contribution of coarse particles was found to be 24 % for total Fe and 23 % for total Al in TSPs, even slightly smaller than the average values in spring. This is probably because, for desert-dust aerosol, Fe and Al were enriched in fine particles, while the major component in coarse particles was quartz (Journet et al., 2014); nevertheless, further measurements are needed to better understand the size distribution of trace metals in desert-dust aerosol.

Compared to other seasons, total Fe concentrations in fine and coarse particles were lowest in summer (Fig. 1a), as aerosol mass concentrations were also lowest in summer (Sect. 3.1). Similarly, previous measurements on Huaniao Island in the East China Sea (Yang et al., 2020) and over the tropical and subtropical North Atlantic (Chen and Siefert, 2004) also found the lowest total aerosol Fe levels in summer. For the other three seasons (spring, fall and winter), the total Fe in coarse particles was rather similar, while the total Fe in fine particles was highest in spring and lowest in fall. Overall, compared to summer and fall, the total aerosol Fe was higher in spring and winter, when higher aerosol mass concentrations were also observed (Fig. S3).

Total Fe was very well correlated with total Al ($0.87 < r < 0.96$, $p < 0.01$) for both coarse (Fig. S4) and fine particles (Fig. 2) in all four seasons, suggesting desert dust always as the dominant source of total aerosol Fe at Xi'an, regardless of particle size range and seasons. The median Fe/Al values, the mass ratios of total Fe to total Al, were 0.975, 0.926, 1.269 and 0.940 in spring, summer, fall and winter for coarse particles and 0.735, 0.796, 0.870 and 0.744 for fine particles (Fig. S5). Fe/Al was found to be 0.911 and 0.741 for PM_{10} and $PM_{2.5}$ generated using surface soil samples collected over several major deserts in China (Zhang et al., 2014). We found that Fe/Al measured for coarse and fine particles at Xi'an was similar to that reported for desert dust (Zhang et al., 2014); coarse particles in fall might be one exception (Fig. S5), showing slightly higher Fe/Al (median: 1.269) than desert dust.

3.3   Dissolved aerosol Fe

Figure 1b shows the seasonal variation of dissolved aerosol Fe in coarse and fine particles at Xi'an. Dissolved aerosol Fe concentrations were in the ranges of 1.0–17.5, 0.9–22.0, 0.7–42.2 and 0.9–33.8 ng m^{-3} for coarse particles in spring, summer, fall and winter, and the average values were 5.9 ± 4.5, 5.6 ± 4.0, 13.5 ± 12.2 and 14.5 ± 8.3 ng m^{-3}; dissolved aerosol Fe concentrations were in the ranges of 1.1–21.4, 2.6–22.9, 2.1–33.7 and 5.0–89.5 ng m^{-3} for fine particles in spring, summer, fall and winter, and the average values were 10.0 ± 5.5, 9.7 ± 5.6, 16.5 ± 10.1 and 22.7 ± 16.8 ng m^{-3}. Average dissolved Fe concentrations were measured as 7.7 ± 14.5 and 7.3 ± 7.6 ng m^{-3} for coarse and fine particles in winter at Qingdao (Zhang et al., 2022), only 53 % and 32 % of the average values (14.5 ± 8.3 and 22.7 ± 16.8 ng m^{-3}) found in winter at Xi'an by the present work, and one major reason is that total Fe concentrations were significantly higher at Xi'an than Qingdao.

The average contributions of coarse particles to dissolved Fe in TSP were 37 %, 36 %, 45 % and 39 % in spring, summer, fall and winter. Compared to fine particles, dissolved Fe was significantly lower in coarse particles for all four seasons (paired t test, $p < 0.01$, $\alpha = 0.05$) at Xi'an, although the total Fe in coarse particles was higher than or similar to fine particles (except spring, as discussed in Sect. 3.2). This indicated that aerosol Fe solubility was lower in coarse particles than fine particles, as further discussed in Sect. 4. Similar to our work, Sakata et al. (2022) found that, over the Pacific, dissolved aerosol Fe concentrations in fine particles (< 1.3 μm) were significantly higher than coarse particles (> 1.3 μm).

Compared to spring and summer, dissolved Fe concentrations were higher in fall and winter for coarse particles (Fig. 1b); for fine particles, dissolved Fe concentrations were highest in winter, followed by fall, and lowest in spring and summer. Dissolved Fe concentrations were low in summer, as total Fe concentrations were also low (Fig. 1a). Total Fe concentrations were high in spring (Fig. 1a), but dissolved

Fe concentrations were low; this is because, compared to other seasons, spring was most severely affected by desert dust with low Fe solubility. Our previous study (Zhang et al., 2022) investigated aerosol Fe at Qingdao in winter and found that, compared to clean days, dissolved Fe concentrations did not change significantly during dust days, although total Fe concentrations were remarkably increased. Therefore, our previous (Zhang et al., 2022) and current studies imply that the occurrence of desert-dust aerosol may not necessarily lead to an increase in dissolved Fe concentrations in the air.

As shown in Fig. S6, overall the correlation between dissolved Fe and total Al was quite weak at Xi'an, indicating that desert dust may not contribute dominantly to dissolved aerosol Fe, although it was always the major source of total aerosol Fe (Sect. 3.2). We also examined correlations between dissolved Fe and several other species (Table S3). Except for summer, dissolved Fe was well correlated with secondary inorganic species (sulfate, nitrate and ammonium) for coarse and fine particles, suggesting secondary formation (i.e., conversion of insoluble Fe to dissolved Fe via chemical processing) as an important source of dissolved Fe. In addition, Fig. 3 shows that dissolved Fe was well correlated with K^+ (a tracer for biomass burning) in coarse and fine particles in all four seasons ($0.67 < r < 0.96$, $p < 0.001$), and this may indicate biomass burning also as an important source of dissolved aerosol Fe.

Furthermore, good correlations with dissolved Fe were found in coarse particles for Pb, Zn and As in three seasons (spring, fall and winter) and in fine particles for Pb (spring, fall and winter), As (spring and fall) and Zn (fall). Aerosol Pb and Zn are mainly emitted by vehicles and the iron–steel industry (Chow et al., 2004; Cao and Cui, 2021), and the major sources of aerosol As include coal combustion and metal smelting (Tian et al., 2010). As a result, vehicle emission, coal combustion, the iron–steel industry and metal smelting also contributed to dissolved aerosol Fe at Xi'an.

4   Aerosol Fe solubility

4.1   Seasonal variation of Fe solubility

4.1.1   Seasonal variability

Figure 4 and Table A1 display aerosol Fe solubility at Xi'an in different seasons. Fe solubility was in the ranges of 0.08 %–2.48 %, 0.13 %–2.44 %, 0.05 %–3.55 % and 0.09 %–7.16 % for coarse particles in spring, summer, fall and winter, and the median values were 0.38 %, 0.51 %, 0.62 % and 0.79 %; for fine particles, Fe solubility was in the ranges of 0.06 %–1.26 %, 0.34 %–3.02 %, 0.27 %–3.37% and 0.21 %–9.65 % in spring, summer, fall and winter, and the median values were 0.42 %, 1.35 %, 1.79 % and 1.17 %.

No significant difference in Fe solubility was found between coarse and fine particles at Xi'an in spring (paired t
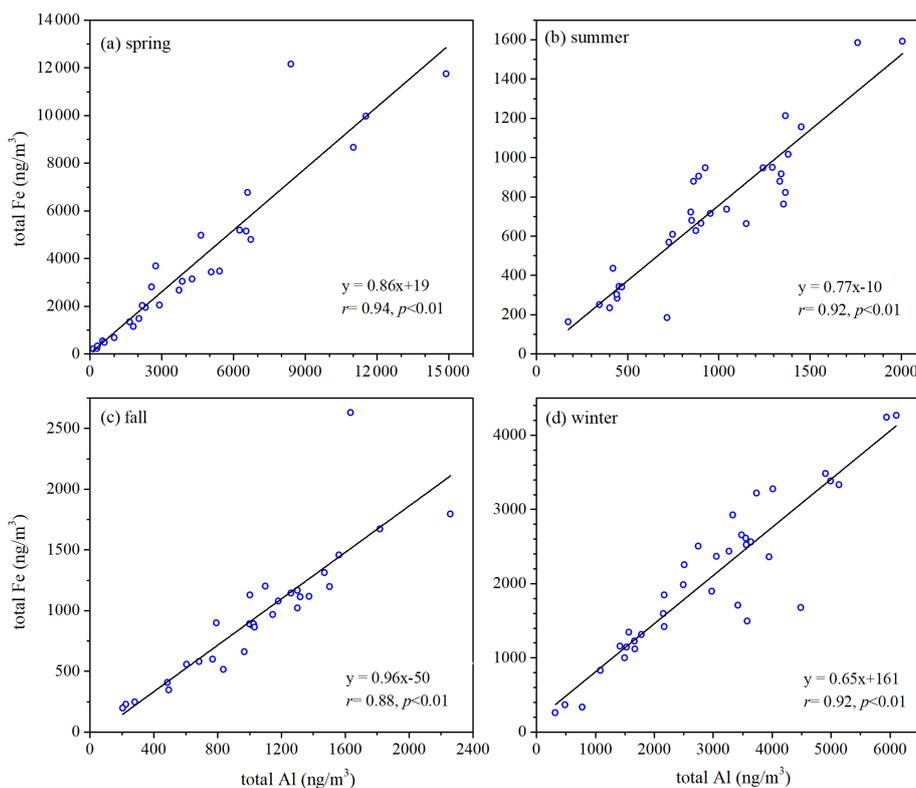
Figure 2. Total Fe versus total Al for fine particles in different seasons: **(a)** spring; **(b)** summer; **(c)** fall; **(d)** winter.

test, $p = 0.17$, $\alpha = 0.05$). In addition, the median values of Fe solubility were both $< 0.5\%$ for coarse and fine particles in spring, similar to desert dust (Schroth et al., 2009; Shi et al., 2011b; Oakes et al., 2012b; Li et al., 2022), and this was because Xi'an was frequently affected by desert-dust aerosol in spring. In the other three seasons (summer, fall and winter), Fe solubility was significantly higher in fine particles than coarse particles (paired t test, $p < 0.01$, $\alpha = 0.05$); furthermore, in these three seasons the median Fe solubility was $> 1\%$ for fine particles and $> 0.5\%$ for coarse particles. For coarse particles, Fe solubility was highest in winter and lowest in spring, while no significant difference was found between summer and fall (t test, $p = 0.95$, $\alpha = 0.05$); for fine particles, Fe solubility can be described by the following order: fall $>$ summer $>$ winter $>$ spring.

A number of field measurements (Hsu et al., 2005; Baker and Jickells, 2006; Sedwick et al., 2007; Kumar et al., 2010; Sholkovitz et al., 2012; Winton et al., 2015; Shelley et al., 2018; Yang et al., 2023) found inverse dependence of Fe solubility on total Fe (and Al). As shown in Figs. 5 and S7, Fe solubility was also observed in our work to decrease with total Fe for coarse and fine particles in three seasons (spring, summer and winter), and such dependence can be fitted using Eq. (1):

$$f_s(\mathrm{Fe}) = a \times [\mathrm{Fe}]_T^{-b}, \qquad (1)$$

where $f_s(\mathrm{Fe})$ is Fe solubility, $[\mathrm{Fe}]_T$ is total Fe concentration, and b represents the sensitivity of Fe solubility to relative change in total Fe concentration. As shown in Figs. S8–S9, such inverse dependence was also observed between Fe solubility and total Al in these three seasons. Several mechanisms can qualitatively explain such inverse dependence, but a consensus has not been reached yet (Mahowald et al., 2018; Meskhidze et al., 2019).

However, no obvious relationship between Fe solubility and total Fe (or total Al) was found in fall. Such inverse dependence was not found in some previous studies either (Paris et al., 2010; Oakes et al., 2012a) and was found for fine particles but not for coarse particles at Qingdao in the winter by our previous work (Zhang et al., 2022). Therefore, one may conclude that the inverse dependence of Fe solubility on total Fe (or total Al), though frequently observed, is not a universal rule. It is not clear yet why such inverse dependence was not observed in these studies.

A larger b value means that Fe solubility is more sensitive to a relative change in the total Fe concentration. For our measurements conducted at Xi'an, b values were determined to be 0.30, 0.23 and 0.91 in spring, summer and winter for fine particles (Fig. S7) and 0.52, 0.65 and 1.16 for coarse particles (Fig. 5). One can see that the b values in winter were much larger than those in spring and summer for both fine and coarse particles; furthermore, in each of the three
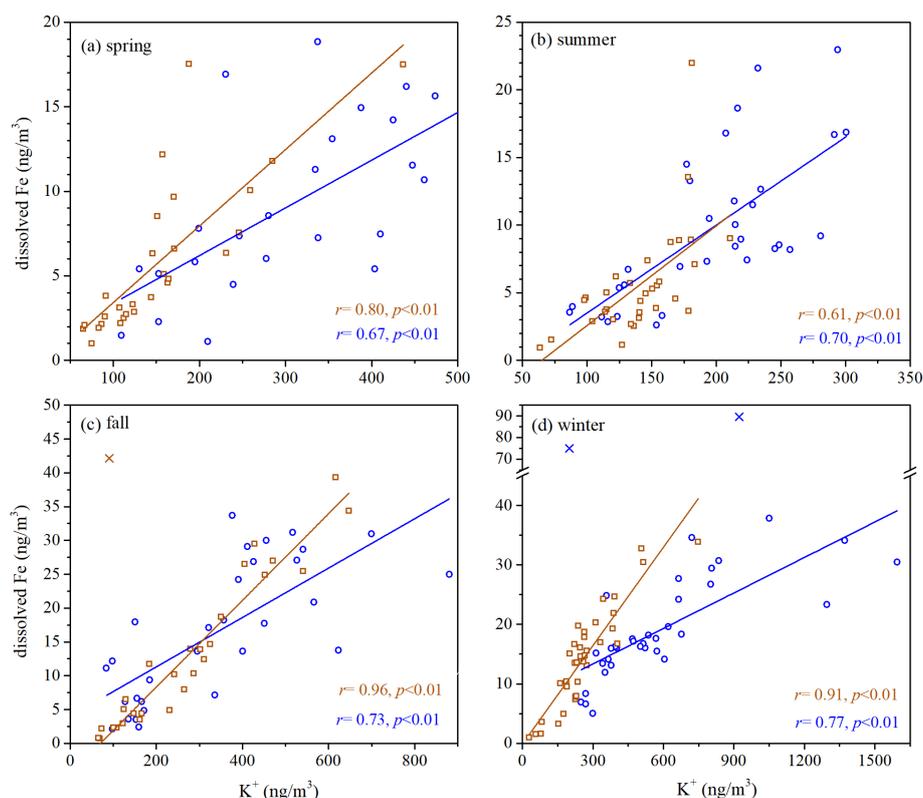
Figure 3. Dissolved Fe versus K^+ for fine and coarse particles in different seasons: **(a)** spring; **(b)** summer; **(c)** fall; **(d)** winter. Blue symbols represent fine particles, and brown symbols represent coarse particles. Cross symbols represent data points which are not included in fittings.
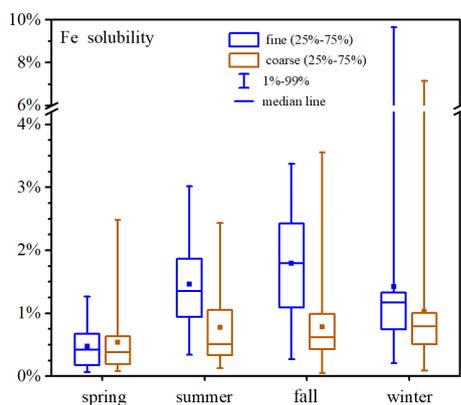
Figure 4. Seasonal variations of aerosol Fe solubility for fine and coarse particles at Xi'an.

seasons (spring, summer and winter), the b value was larger for coarse particles than fine particles.

4.1.2 Comparison with previous work

The median Fe solubility at Xi'an was 0.79 % and 1.17 % for coarse and fine particles in winter, larger than those (0.34 % and 0.66 %, respectively) found in winter at Qingdao (Zhang et al., 2022). One reason is that in winter Xi'an was fre-

quently affected by haze pollution when aerosol Fe solubility was significantly increased (Shi et al., 2020; Zhang et al., 2022; Zhu et al., 2022); in addition, our winter sampling at Qingdao was severely affected by desert-dust aerosol (Zhang et al., 2022), with very-low Fe solubility.

Several previous studies also investigated aerosol Fe solubility in northern China. Similar to our current work, Chuang et al. (2005) reported low Fe solubility (< 1 %) for TSPs during spring at Dunhuang, a city in northwestern China. Average Fe solubility at Xi'an was reported to be 10.4 % for TSPs (He et al., 2021) and 25.5 ± 11.3 % for $PM_{2.5}$ (Lei et al., 2023), 5.0 ± 3.8 %, 4.5 ± 2.6 % and 2.7 ± 1.5 % for $PM_{2.5}$ at three cities in northern China (Zhu et al., 2020) and 2.70 ± 2.77 % for TSPs at Qingdao (Shi et al., 2020). Compared to our work, some other studies (Shi et al., 2020; Zhu et al., 2020; He et al., 2021; Lei et al., 2023) reported higher Fe solubility, mainly because different leaching protocols were employed to extract dissolved Fe (Meskhidze et al., 2019; Li et al., 2023): (1) sonication was used during extraction in three previous studies (Shi et al., 2020; Zhu et al., 2020; He et al., 2021), but not in our work; (2) the filter pore size Shi et al. (2020) used (0.45 µm) was larger than that our work used (0.22 µm); (3) the leaching solution used by Lei et al. (2023) (acetate buffer, pH = 4.3) was more acidic than that we used (ultrapure water).
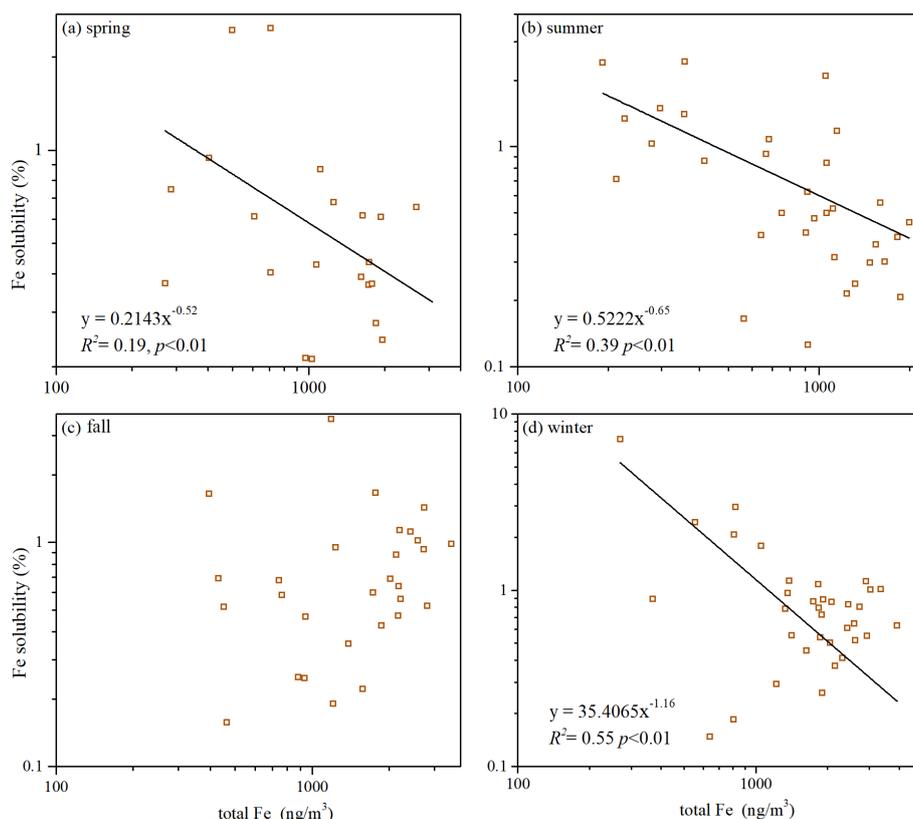
Figure 5. Fe solubility versus total Fe for coarse particles in different seasons: **(a)** spring; **(b)** summer; **(c)** fall; **(d)** winter.

4.1.3 Fe solubility during dust and haze events

At Xi'an, dust events ($PM_{10} > 100 \mu g\,m^{-3}$ and $PM_{10} / PM_{2.5} > 3$) occurred in spring (12–17 and 27–30 April). During the two dust events, average Fe solubility was $0.17 \pm 0.09\%$ and $0.18 \pm 0.13\%$ for coarse and fine particles, similar to that reported for dust particles collected from dust source regions (Shi et al., 2011b; Oakes et al., 2012b; Paris and Desboeufs, 2013; Li et al., 2022); during non-dust periods in spring, average Fe solubility was found to be $0.75 \pm 0.66\%$ and $0.64 \pm 0.27\%$ for coarse and fine particles, higher than that observed for dust events. In fact, much lower Fe solubility was also reported during dust events at Qingdao (Shi et al., 2020; Zhang et al., 2022), Jeju Island (Chuang et al., 2005) and Hokkaido (Ooki et al., 2009) when compared to non-dust periods.

In this work we classified high-RH haze events as those with $PM_{2.5} > 80 \mu g\,m^{-3}$, $PM_{2.5} / PM_{10} > 0.8$ and $RH > 80\%$. High-RH haze events at Xi'an only occurred in winter (26 November–1 December and 5–7 December). Average Fe solubility was measured as $2.03 \pm 2.07\%$ and $2.16 \pm 2.81\%$ for coarse and fine particles during high-RH haze events, significantly higher than that observed for other days in winter ($0.69 \pm 0.46\%$ and $1.18 \pm 0.81\%$ on average, respectively). Some previous studies (Shi et al., 2020; Zhu et al., 2020, 2022; Zhang et al., 2022) also observed evaluated

aerosol Fe solubility during haze periods, attributed to increased contribution of anthropogenic Fe with high solubility and/or Fe solubility enhancement via chemical processing.

4.2 Influence of air mass sources on Fe solubility

Back trajectories obtained for our campaign were clustered, and we further examined the dependence of Fe solubility on air mass cluster types in different seasons. In spring (Fig. 6a), air mass cluster C1 originated locally, and C2 originated from the North China Plain with severe air pollution, while C3 and C4 represented air mass arriving from desert regions in the north and northwest after long-distance transport (compared to C1 and C2); as shown in Fig. 6b, Fe solubility in coarse and fine particles was significantly higher for C1 and C2 when compared to C3 and C4.

In fall (Fig. 6e), air mass cluster C1 originated locally, C2 was transported from desert regions in the north and northwest, and Fe solubility was much higher for C1 than C2 (Fig. 6f). In winter (Fig. 6g), air mass cluster C1 originated locally, while C2, C3 and C4 originated from desert regions in the north and northwest, and the transport distance increased from C2 to C4; as shown in Fig. 6h, Fe solubility followed the order C1 > C2 > C3 > C4, decreasing with an increase in transport distance. In contrast to the other three

seasons, no obvious dependence of Fe solubility on air mass clusters was found in summer (Fig. 6d).

To summarize, our work found that, in spring, fall and winter, Fe solubility at Xi'an was significantly higher when air masses originated from local and nearby regions when compared to those arriving from desert regions after long-distance transport. The reason is that the contribution of anthropogenic emissions to aerosol Fe was elevated for air masses originating from local and nearby sources (when compared to air masses originating from desert regions), and anthropogenic aerosol Fe had higher solubility than desert dust (Schroth et al., 2009; Fu et al., 2012; Oakes et al., 2012b). Similar to our work, over the Sargasso Sea aerosol Fe solubility was much lower in Saharan air masses than North American air masses (Sedwick et al., 2007).

4.3 Effects of chemical aging

Laboratory studies (Shi et al., 2011a; Chen and Grassian, 2013; Wang et al., 2018) suggested that chemical processing by acids, such as H_2SO_4 and HNO_3, could dissolve insoluble Fe and thus enhance aerosol Fe solubility. Some field studies found that aerosol Fe solubility was positively correlated with sulfate and/or nitrate (Shi et al., 2020; Zhu et al., 2020; Liu et al., 2021; Zhang et al., 2022; Yang et al., 2023), indicating enhancement of Fe solubility by atmospheric acid processing.

Figure 7 plots Fe solubility at Xi'an versus $(2 \times [\text{sulfate}] + [\text{nitrate}]) / [\text{Fe}]$ (in nanomole per nanomole, referred to as relative abundance of aerosol acidic species), the molar ratio of two major acidic species to total Fe in aerosol particles. For coarse particles, aerosol Fe solubility was well correlated with relative abundance of aerosol acidic species in all four seasons ($0.77 < r < 0.91$, $p < 0.01$). For fine particles, good correlation was found in spring ($r = 0.84$, $p < 0.01$), moderate correlation was found in fall and winter ($0.42 < r < 0.53$, $p < 0.01$), and no significant correlation was found in summer ($r = 0.35$, $p > 0.05$). In addition, as shown in Figs. S10–S11, correlations of Fe solubility with [nitrate] / [Fe] were better than (or very similar to) those with [sulfate] / [Fe] for coarse particles in the four seasons, whereas no obvious trend was observed for fine particles.

Overall, correlations between Fe solubility and relative abundance of aerosol acidic species were always better for coarse particles than fine particles (Fig. 7), indicating that acid processing may be more important in Fe solubility enhancement for coarse particles when compared to fine particles. A previous study (Zhang et al., 2022) also found that such correlation was better in coarse particles than fine particles in winter at Qingdao, a coastal city in northern China. Nevertheless, as discussed in Sect. 4.1, Fe solubility was higher in fine particles than coarse particles. This may imply that primary emission of non-desert-dust Fe (anthropogenic Fe) with higher solubility (Schroth et al., 2009; Oakes et al.,

2012b) was more important for Fe solubility enhancement in fine particles than coarse particles.

It was suggested by laboratory studies (Chen and Grassian, 2013; Paris and Desboeufs, 2013; Wang et al., 2017) that atmospheric organic ligands, such as oxalate, could increase aerosol Fe solubility via ligand-promoted dissolution. As shown in Fig. S12, our present work found good correlation between Fe solubility with [oxalate] / [Fe] (in nanomole per nanomole) for coarse particles ($0.70 < r < 0.88$, $p < 0.01$) and moderate correlation for fine particles ($0.40 < r < 0.67$, $p < 0.01$) at Xi'an. Positive correlation between Fe solubility and oxalate was also observed previously in Atlanta, USA (Yang and Weber, 2022), Toronto, Canada (Tao et al., 2022), and Qingdao, China (Zhang et al., 2022).

We note that good correlation between Fe solubility and aerosol oxalate does not necessarily mean Fe solubility enhancement by Fe–oxalate complexation. For example, it was suggested that Fe could promote the formation of oxalate in aerosol particles (Tao and Murphy, 2019; Zhang et al., 2019), and thus good correlation between Fe solubility and oxalate could also imply enhanced formation of oxalate by dissolved Fe. In addition, similar to sulfate and nitrate, the major source of oxalate in the troposphere was secondary formation (Myriokefalitakis et al., 2011; Kawamura and Bikkina, 2016), and in this aspect good correlation between Fe solubility and relative abundance of oxalate could also indicate the importance of secondary formation of dissolved aerosol Fe (i.e., dissolution of insoluble Fe to dissolved Fe via aging processes).

5 Discussion: roles of RH and aerosol acidity

Figure 8 reveals the importance of RH in regulating aerosol Fe solubility. When RH was increased from < 60 % to 60 %–70 %, a significant increase in Fe solubility was observed for both coarse and fine particles. Sun et al. (2018) investigated hygroscopicity of aerosol particles collected in northern China and found that most particles examined started to become deliquesced when RH was increased to ∼ 60 %. The deliquescenced RH reported for ambient aerosol particles (Sun et al., 2018) coincided roughly with the RH threshold at which a large increase in aerosol Fe solubility was observed in our work. Previous studies (Shi et al., 2020; Zhu et al., 2020, 2022) also highlighted that RH and thus aerosol liquid water could substantially affect Fe solubility. For example, Zhu et al. (2020) measured Fe solubility at four cities in eastern China in December 2017 and found that Fe solubility at > 50 % RH was significantly larger than that at < 50 % RH.

In addition, as shown in Fig. 8, when RH was increased from 80 %–90 % to > 90 %, median Fe solubility remarkably increased from 0.67 % to 1.68 % for coarse particles. Similarly to our work, Shi et al. (2020) also found that aerosol Fe solubility at Qingdao was significantly increased under foggy weather when compared to other weather conditions. There-
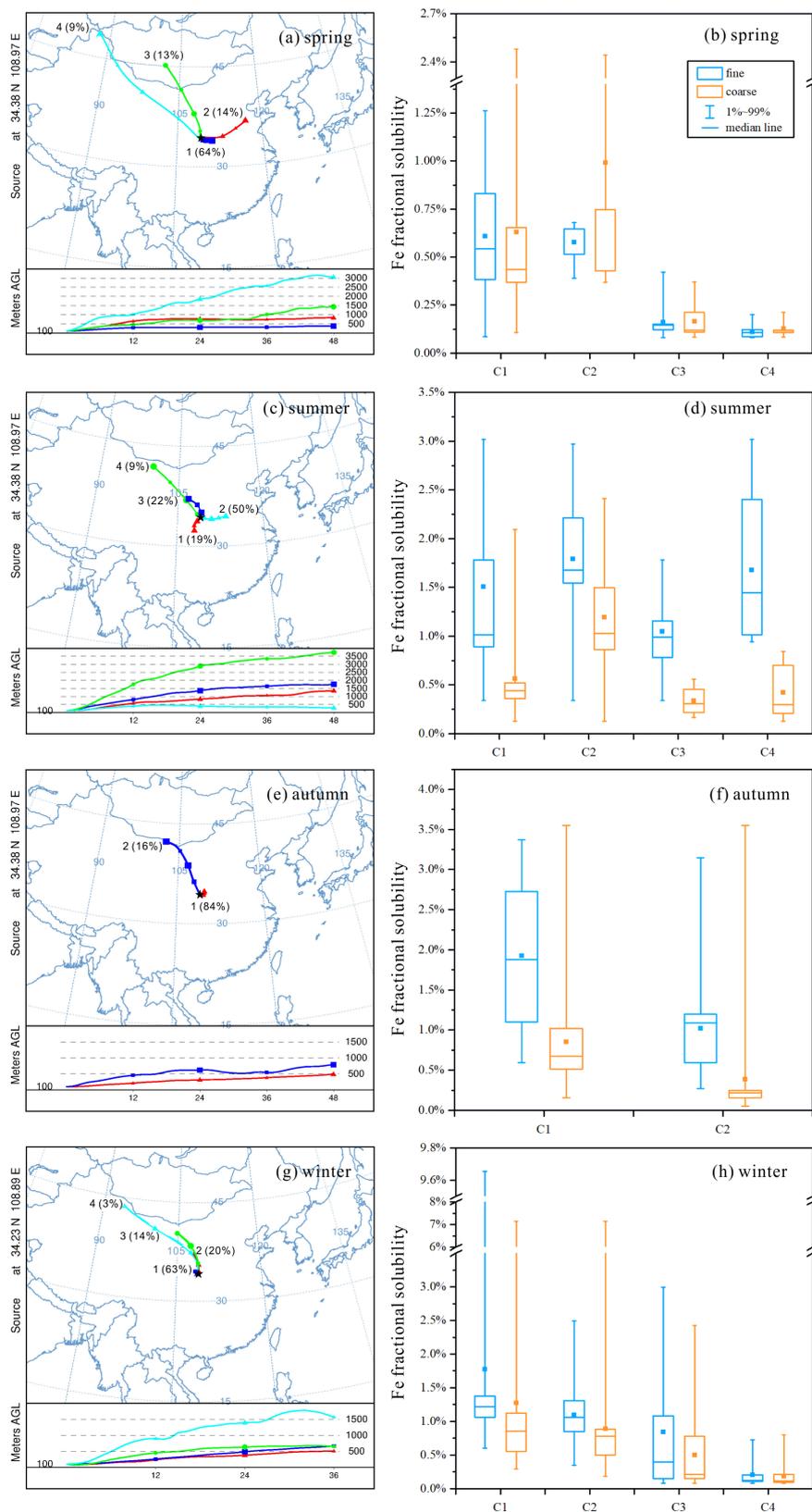
Figure 6. The mean back-trajectory clusters obtained by HYSPLIT for **(a)** spring, **(c)** summer, **(e)** fall, and **(g)** winter; Fe solubility in fine and coarse particles for different air mass clusters in **(b)** spring, **(d)** summer, **(f)** fall, and **(h)** winter. C1–C4 represent different air mass clusters.
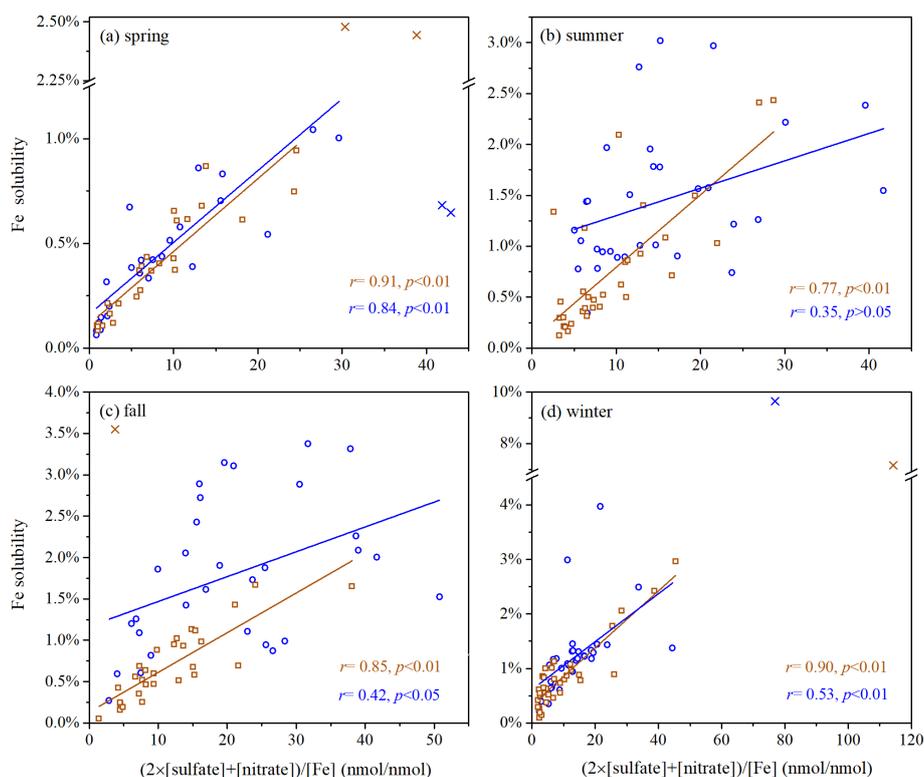
Figure 7. Fe solubility versus $(2 \times [\text{sulfate}] + [\text{nitrate}]) / [\text{Fe}]$ for fine and coarse particles in different seasons: **(a)** spring; **(b)** summer; **(c)** fall; **(d)** winter. Blue symbols represent fine particles, and brown symbols represent coarse particles. Cross symbols represent data points which are not included in fittings.
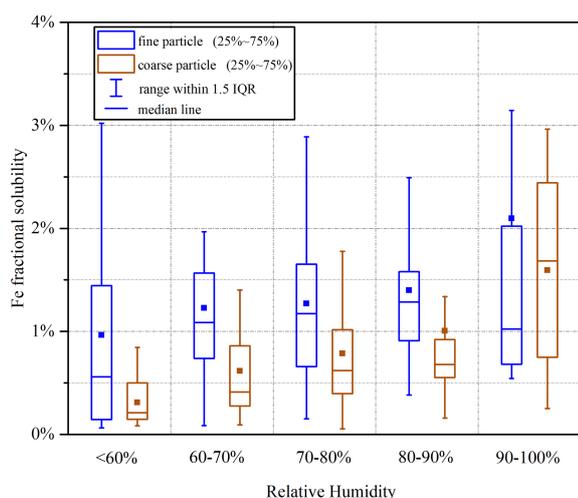
Figure 8. Fe solubility in different RH (relative humidity) ranges for fine and coarse particles (RH < 60 %: 18 d; 60 % < RH < 70 %: 23 d; 70 % < RH < 80 %: 48 d; 80 % < RH < 90 %: 28 d; RH > 90 %: 10 d).

fore, both Shi et al. (2020) and our present work suggested that high RH could promote Fe dissolution.

We further examined the impact of aerosol acidity on Fe solubility, and the results are displayed in Fig. 9. For coarse particles, an increase in pH did not lead to an apparent change in Fe solubility as long as aerosol pH was < 5; however, Fe solubility was greatly decreased when aerosol pH was increased to > 5. For fine particles, Fe solubility in general decreased with increasing aerosol pH (from < 2 to > 5). Previous work carried out at six Canadian sites (Tao and Murphy, 2019) and Atlanta, USA (Wong et al., 2020; Yang and Weber, 2022), also reported higher Fe solubility at lower aerosol pH. Similar to our previous work at Qingdao in the winter (Zhang et al., 2022), our current study found that, for coarse and fine particles at Xi'an, aerosol pH was mostly < 4 when Fe solubility exceeded 1 % (Fig. S13). It should be pointed out that for some samples collected at Xi'an, Fe solubility could still be very low (< 1 %), even when aerosol pH was low and RH was high (Fig. S13). In total, 34 samples for coarse particles (9 in spring, 8 in summer, 12 in fall and 5 in winter) and 18 samples for fine particles (7 in spring, 6 in summer, 4 in fall and 1 in winter) fulfilled the above conditions (pH < 4, RH > 80 % and Fe solubility < 1 %). Fe mineralogy may possibly explain the observed low Fe solubility
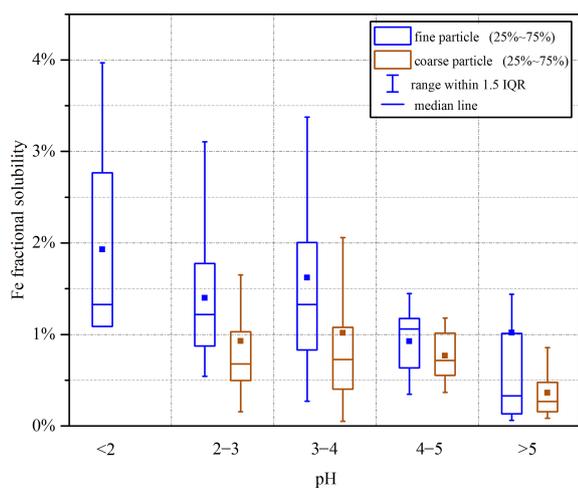
Figure 9. Fe solubility in different pH ranges for fine and coarse particles at Xi'an.

despite high RH and aerosol acidity, and concurrent measurements of Fe mineralogy could provide further clues.

In addition, as shown in Fig. 9, at a given pH range, Fe solubility was always higher in fine particles than coarse particles. If we assume at the same pH range that Fe solubility enhancement by acid processing was similar for fine and coarse particles, the results displayed in Fig. 9 may imply that anthropogenic and pyrogenic Fe played a more important role in Fe solubility enhancement in fine particles at Xi'an when compared to coarse particles. Mcdaniel et al. (2019) found that soluble Fe concentration was strongly correlated with aerosol surface area for size-resolved aerosol samples collected from several different regions and suggested surface area as the main factor which affected Fe solubility; they further suggested that this was because Fe solubility enhancement by acid processing could be more effective for aerosol particles with larger surface areas and thus smaller particle sizes.

Our work found that at Xi'an aerosol pH values for both coarse and fine particles were lower (t test, $p < 0.01$, $\alpha = 0.05$) in summer and fall than in spring and winter (Table S4 and Fig. S14). Compared to summer and fall, lower temperature in winter favored partitioning of ammonium in aerosol particles and thus led to higher aerosol pH. Average temperatures were similar in spring and fall at Xi'an (Table S1), but aerosol pH was higher in spring than in fall (Table S4). Higher aerosol pH in spring at Xi'an, when compared to fall, was caused by an increase in non-volatile cations in spring due to the influence of desert-dust aerosol; in fact, we found that the abundance of Ca^{2+} (relative to sulfate) was much higher in spring for both fine and coarse particles. Meanwhile, Fe solubility was higher in summer (median: 1.35 %) and fall (median: 1.79 %) than in spring (median: 0.42 %) and winter (median: 1.17 %) for fine particles and was also higher in summer (median: 0.51 %) and fall (median: 0.62 %)

than in spring (median: 0.38 %) for coarse particles. As a result, lower aerosol pH (and thus higher aerosol acidity) in summer and fall may at least partly explain the observed higher Fe solubility in these two seasons. Our results were corroborated by a previous study (Yang and Weber, 2022), which found that, compared to the cold season, higher Fe solubility was found in Atlanta (Georgia, USA) in the warm season when aerosol pH was lower.

6   Summary and conclusion

Our work investigated total Fe, dissolved Fe and Fe solubility for coarse ($> 1 \mu m$) and fine ($< 1 \mu m$) particles in four different seasons at Xi'an, a megacity in northwestern China impacted by anthropogenic emissions and desert dust. Total Fe concentrations in coarse particles were lowest in summer and similar in the other three seasons, while for fine particles total Fe concentrations were lowest in summer and highest in spring. Good correlations were found between total Fe and total Al for both coarse and fine particles in all four seasons, suggesting desert-dust aerosol as the major source of total Fe regardless of particle size (below or above 1 μm) and season.

Dissolved Fe concentrations were higher in fall and winter than in spring and summer for coarse particles; for fine particles, dissolved Fe concentrations were highest in winter, followed by fall, and lowest in spring and summer. Compared to the other seasons, although total Fe concentrations were evaluated in spring due to the impacts of desert dust, an increase in dissolved Fe levels was not observed. This may imply that the occurrence of desert-dust aerosol may not necessarily lead to an increase in dissolved Fe concentrations, as also revealed in our previous study (Zhang et al., 2022) carried out at a coastal city in northern China. Dissolved Fe was significantly lower for coarse particles (compared to fine particles) in all four seasons, although the total Fe in coarse particles was higher than or similar to fine particles in three seasons (but not spring), implying higher Fe solubility in fine particles. Overall, the correlation between dissolved Fe and total Al was rather weak, suggesting that desert dust may not contribute dominantly to dissolved Fe at Xi'an, although it was always the major source of total Fe.

The highest Fe solubility was observed in winter for coarse particles and in fall for fine particles; meanwhile, the lowest Fe solubility was observed in spring for both coarse and fine particles, with the median Fe solubility below 0.5 %. Compared to coarse particles, Fe solubility was similar for fine particles in spring but significantly higher in the other three seasons. Inverse dependence of Fe solubility on total Fe concentration was observed for coarse and fine particles in spring, summer and winter, while there was no such dependence for either fine or coarse particles in fall. Furthermore, aerosol Fe solubility was higher in air masses originating from local and nearby regions than those arriving from desert regions after long-distance transport in three seasons

(spring, fall and winter), while no apparent dependence of Fe solubility on air mass origins was found in summer.

Our work found better correlation between Fe solubility and relative abundance of aerosol acidic species for coarse particles than fine particles in all four seasons, probably suggesting that acid processing was more important for Fe solubility enhancement in coarse particles. This may further mean that non-desert-dust Fe (e.g., anthropogenic and biomass burning Fe) was more important for Fe solubility enhancement in fine particles, since Fe solubility was higher in fine particles than coarse particles. We also found that overall Fe solubility increased with RH and acid acidity for coarse and fine particles, underscoring the importance of aerosol liquid water and aerosol acidity in enhancing Fe solubility via acid processing. Our work further found that at a given pH range aerosol Fe solubility was always higher in fine particles than coarse particles.

Appendix A

Table A1. Overview of total Fe ($ng\,m^{-3}$), dissolved Fe ($ng\,m^{-3}$) and Fe solubility (%) for fine and coarse particles in different seasons at Xi'an.

	Fine particles			Coarse particles		
Spring	Range	Median	Average	Range	Median	Average
Total Fe	206–12 144	2925	3717 ± 3387	270–3095	1626	1504 ± 800
Dissolved Fe	1.1–21.4	9.2	10.0 ± 5.5	1.0–17.5	4.2	5.9 ± 4.5
Fe solubility	0.06–1.26	0.42	0.48 ± 0.32	0.08–2.48	0.38	0.54 ± 0.59
Summer	Range	Median	Average	Range	Median	Average
Total Fe	164–1591	719	721 ± 366	191–1992	942	950 ± 524
Dissolved Fe	2.6–22.9	8.5	9.7 ± 5.6	0.9–22.0	4.6	5.6 ± 4.0
Fe solubility	0.3–3.02	1.35	1.46 ± 0.67	0.13–2.44	0.51	0.78 ± 0.63
Fall	Range	Median	Average	Range	Median	Average
Total Fe	196–2631	934	958 ± 516	395–3492	1651	1638 ± 830
Dissolved Fe	2.1–33.7	15.4	16.5 ± 10.1	0.7–42.2	10.3	13.5 ± 12.2
Fe solubility	0.27–3.37	1.79	1.80 ± 0.88	0.05–3.55	0.62	0.79 ± 0.67
Winter	Range	Median	Average	Range	Median	Average
Total Fe	257–4268	1942	2058 ± 1037	269–3924	1850	1831 ± 866
Dissolved Fe	5.0–89.5	17.4	22.7 ± 16.8	0.9–33.8	14.7	14.5 ± 8.3
Fe solubility	0.21–9.65	1.17	1.43 ± 1.58	0.09–7.16	0.79	1.03 ± 1.22

References

Abbaspour, N., Hurrell, R., and Kelishadi, R.: Review on iron and its importance for human health, J. Res. Med. Sci., 19, 164–174, 2014.

Alexander, B., Park, R. J., Jacob, D. J., and Gong, S. L.: Transition metal-catalyzed oxidation of atmospheric sulfur: Global implications for the sulfur budget, J. Geophys. Res.-Atmos., 114, D02309, https://doi.org/10.01029/02008jd010486, 2009.

Baker, A. R. and Jickells, T. D.: Mineral particle size as a control on aerosol iron solubility, Geophys. Res. Lett., 33, L17608, https://doi.org/10.11029/12006GL026557, 2006.

Baker, A. R., Kanakidou, M., Nenes, A., Myriokefalitakis, S., Croot, P. L., Duce, R. A., Gao, Y., Guieu, C., Ito, A., Jickells, T. D., Mahowald, N. M., Middag, R., Perron, M. M. G., Sarin, M. M., Shelley, R., and Turner, D. R.: Changing atmospheric acidity as a modulator of nutrient deposition and ocean biogeochemistry, Sci. Adv., 7, eabd8800, https://doi.org/10.1126/sciadv.abd8800, 2021.

Baker, J.: A cluster analysis of long range air transport pathways and associated pollutant concentrations within the UK, Atmos. Environ., 44, 563–571, 2010.

Boyd, P. W. and Ellwood, M. J.: The biogeochemical cycle of iron in the ocean, Nat. Geosci., 3, 675–682, 2010.

Cao, J. J. and Cui, L.: Current Status, Characteristics and Causes of Particulate Air Pollution in the Fenwei Plain, China: A Review, J. Geophys. Res.-Atmos, 126, e2020JD034472, https://doi.org/10.1029/2020JD034472, 2021.

Cao, J. J., Wang, Q. Y., Chow, J. C., Watson, J. G., Tie, X. X., Shen, Z. X., Wang, P., and An, Z. S.: Impacts of aerosol compositions on visibility impairment in Xi'an, China, Atmos. Environ., 59, 559–566, 2012.

Chen, H. H. and Grassian, V. H.: Iron Dissolution of Dust Source Materials during Simulated Acidic Processing: The Effect of Sulfuric, Acetic, and Oxalic Acids, Environ. Sci. Tech., 47, 10312–10321, 2013.

Chen, Y. and Siefert, R. L.: Seasonal and spatial distributions and dry deposition fluxes of atmospheric total and labile iron over the tropical and subtropical North Atlantic Ocean, J. Geophys. Res.-Atmos, 109, D09305, https://doi.org/10.01029/02003JD003958, 2004.

Chen, Q. C., Hua, X. Y., Li, J. W., Chang, T., and Wang, Y. Q.: Diurnal evolutions and sources of water-soluble chromophoric aerosols over Xi'an during haze event, in Northwest China, Sci. Total Environ., 786, 147412, https://doi.org/10.1016/j.scitotenv.2021.147412, 2021.

Chow, J. C., Watson, J. G., Kuhns, H., Etyemezian, V., Lowenthal, D. H., Crow, D., Kohl, S. D., Engelbrecht, J. P., and Green, M. C.: Source profiles for industrial, mobile, and area sources in the Big Bend Regional Aerosol Visibility and Observational study, Chemosphere, 54, 185–208, 2004.

Chuang, P. Y., Duvall, R. M., Shafer, M. M., and Schauer, J. J.: The origin of water soluble particulate iron in the Asian atmospheric outflow, Geophys. Res. Lett., 32, L07813, https://doi.org/10.01029/02004GL021946, 2005.

Ding, J., Zhao, P., Su, J., Dong, Q., Du, X., and Zhang, Y.: Aerosol pH and its driving factors in Beijing, Atmos. Chem. Phys., 19, 7939–7954, https://doi.org/10.5194/acp-19-7939-2019, 2019.

Draxier, R. R. and Hess, G. D.: An overview of the HYSPLIT_4 modelling system for trajectories, dispersion and deposition, Aust. Meteorol. Mag., 47, 295–308, 1998.

Fang, T., Guo, H. Y., Zeng, L. H., Verma, V., Nenes, A., and Weber, R. J.: Highly Acidic Ambient Particles, Soluble Metals, and Oxidative Potential: A Link between Sulfate and Aerosol Toxicity, Environ. Sci. Technol., 51, 2611–2620, 2017.

Fountoukis, C. and Nenes, A.: ISORROPIA II: a computationally efficient thermodynamic equilibrium model for K^+-Ca^{2+}-Mg^{2+}-NH_4^+-Na^+-SO_4^{2-}-NO_3^--Cl^--H_2O aerosols, Atmos. Chem. Phys., 7, 4639–4659, https://doi.org/10.5194/acp-7-4639-2007, 2007.

Fu, H. B., Lin, J., Shang, G. F., Dong, W. B., Grassian, V. H., Carmichael, G. R., Li, Y., and Chen, J. M.: Solubility of Iron from Combustion Source Particles in Acidic Media Linked to Iron Speciation, Environ. Sci. Technol., 46, 11119–11127, 2012.

Guo, H., Xu, L., Bougiatioti, A., Cerully, K. M., Capps, S. L., Hite Jr., J. R., Carlton, A. G., Lee, S.-H., Bergin, M. H., Ng, N. L., Nenes, A., and Weber, R. J.: Fine-particle water and pH in the southeastern United States, Atmos. Chem. Phys., 15, 5211–5228, https://doi.org/10.5194/acp-15-5211-2015, 2015.

Hamilton, D. S., Scanza, R. A., Rathod, S. D., Bond, T. C., Kok, J. F., Li, L., Matsui, H., and Mahowald, N. M.: Recent (1980 to 2015) Trends and Variability in Daily-to-Interannual Soluble Iron Deposition from Dust, Fire, and Anthropogenic Sources, Geophys. Res. Lett., 47, e2020GL089688, https://doi.org/10.1029/2020GL089688, 2020.

He, X., Liu, P., Zhao, W., Xu, H., Zhang, R., and Shen, Z.: Size distribution of water-soluble metals in atmospheric particles in Xi'an, China: Seasonal variations, bioavailability, and health risk assessment, Atmos. Poll. Res., 12, 101090, https://doi.org/10.1016/j.apr.2021.101090, 2021.

Hennigan, C. J., Izumi, J., Sullivan, A. P., Weber, R. J., and Nenes, A.: A critical evaluation of proxy methods used to estimate the acidity of atmospheric particles, Atmos. Chem. Phys., 15, 2775–2790, https://doi.org/10.5194/acp-15-2775-2015, 2015.

Hsu, S.-C., Lin, F.-J., and Jeng, W.-L.: Seawater solubility of natural and anthropogenic metals within ambient aerosols collected from Taiwan coastal sites, Atmos. Environ., 39, 3989–4001, 2005.

Huang, X., Song, Y., Zhao, C., Li, M., Zhu, T., Zhang, Q., and Zhang, X.: Pathways of sulfate enhancement by natural and anthropogenic mineral aerosols in China, J. Geophys. Res.-Atmos, 119, 14165–14179, 2014.

Ito, A., Myriokefalitakis, S., Kanakidou, M., Mahowald, N. M., Scanza, R. A., Hamilton, D. S., Baker, A. R., Jickells, T., Sarin, M., Bikkina, S., Gao, Y., Shelley, R. U., Buck, C. S., Landing, W. M., Bowie, A. R., Perron, M. M. G., Guieu, C., Meskhidze, N., Johnson, M. S., Feng, Y., Kok, J. F., Nenes, A., and Duce, R. A.: Pyrogenic iron: The missing link to high iron solubility in aerosols, Sci. Adv., 5, eaau7671, https://doi.org/10.1126/sciadv.aau7671, 2019.

Ito, A., Ye, Y., Baldo, C., and Shi, Z. B.: Ocean fertilization by pyrogenic aerosol iron, Npj Clim. Atmos. Sci., 4, 30, https://doi.org/10.1038/s41612-41021-00185-41618, 2021.

Jickells, T. D., An, Z. S., Andersen, K. K., Baker, A. R., Bergametti, G., Brooks, N., Cao, J. J., Boyd, P. W., Duce, R. A., Hunter, K. A., Kawahata, H., Kubilay, N., laRoche, J., Liss, P. S., Mahowald, N., Prospero, J. M., Ridgwell, A. J., Tegen, I., and Torres, R.: Global Iron Connections between Desert Dust, Ocean Biogeochemistry, and Climate, Science, 308, 67–71, 2005.

Journet, E., Balkanski, Y., and Harrison, S. P.: A new data set of soil mineralogy for dust-cycle modeling, Atmos. Chem. Phys., 14, 3801–3816, https://doi.org/10.5194/acp-14-3801-2014, 2014.

Kawamura, K. and Bikkina, S.: A review of dicarboxylic acids and related compounds in atmospheric aerosols: Molecular distributions, sources and transformation, Atmos. Res., 170, 140–160, 2016.

Kelly, F. J.: Oxidative stress: Its role in air pollution and adverse health effects, Occup. Environ. Med., 60, 612–616, 2003.

Kumar, A., Sarin, M. M., and Srinivas, B.: Aerosol iron solubility over Bay of Bengal: Role of anthropogenic sources and chemical processing, Mar. Chem., 121, 167–175, 2010.

Lei, Y., Li, D., Lu, D., Zhang, T., Sun, J., Wang, X., Xu, H., and Shen, Z.: Insights into the roles of aerosol soluble iron in secondary aerosol formation, Atmos. Environ., 294, 119507, https://doi.org/10.1016/j.atmosenv.2022.119507, 2023.

Li, R., Zhang, H. H., Wang, F., He, Y. T., Huang, C. P., Luo, L., Dong, S. W., Jia, X. H., and Tang, M. J.: Mass fractions, solubility, speciation and isotopic compositions of iron in coal and municipal waste fly ash, Sci. Total Environ., 838, 155974, https://doi.org/10.1016/j.scitotenv.2022.155974, 2022.

Li, R., Dong, S. W., Huang, C. P., Yu, F., Wang, F., Li, X. F., Zhang, H. H., Ren, Y., Guo, M. X., Chen, Q. C., Ge, B. Z., and Tang, M. J.: Evaluating the effects of contact time and leaching solution on measured solubilities of aerosol trace metals, Appl. Geochem., 148, 105551, https://doi.org/10.1016/j.apgeochem.2022.105551, 2023.

Li, W. J., Xu, L., Liu, X. H., Zhang, J. C., Lin, Y. T., Yao, X. H., Gao, H. W., Zhang, D. Z., Chen, J. M., Wang, W. X., Harrison, R. M., Zhang, X. Y., Shao, L. Y., Fu, P. Q., Nenes, A., and Shi, Z. B.: Air pollution–aerosol interactions produce more bioavailable iron for ocean ecosystems, Science Adv., 3, e1601749, https://doi.org/10.1126/sciadv.1601749, 2017.

Liu, L., Lin, Q., Liang, Z., Du, R., Zhang, G., Zhu, Y., Qi, B., Zhou, S., and Li, W.: Variations in concentration and solubility of iron in atmospheric fine particles during the COVID-19 pandemic: An example from China, Gondwana Res., 97, 138–144, 2021.

Liu, M. X., Matsui, H., Hamilton, D. S., Lamb, K. D., Rathod, S. D., Schwarz, J. P., and Mahowald, N. M.: The underappreciated role of anthropogenic sources in atmospheric soluble iron flux to the Southern Ocean, Npj Clim. Atmos. Sci., 5, 28, 10.1038/s41612-022-00250-w, 2022.

Mahowald, N. M., Hamilton, D. S., Mackey, K. R. M., Moore, J. K., Baker, A. R., Scanza, R. A., and Zhang, Y.: Aerosol trace metal leaching and impacts on marine microorganisms, Nat. Commun., 9, 2614, https://doi.org/10.1038/s41467-018-04970-7, 2018.

Martin, J. H.: Glacial-interglacial CO$_2$ change: the iron hypothesis, Paleoceanography, 5, 1–13, 1990. Martin, L. R. and Good, T. W.: Catalyzed oxidation of sulfur dioxide in solution: The iron-manganese synergism, Atmos. Environ., 25, 2395–2399, 1991.

McDaniel, M. F. M., Ingall, E. D., Morton, P. L., Castorina, E., Weber, R. J., Shelley, R. U., Landing, W. M., Longo, A. F., Feng, Y., and Lai, B.: Relationship between Atmospheric Aerosol Mineral Surface Area and Iron Solubility, ACS Earth Space Chem., 3, 2443–2451, 2019.

Meskhidze, N., Volker, C., Al-Abadleh, H. A., Barbeau, K., Bressac, M., Buck, C., Bundy, R. M., Croot, P., Feng, Y., Ito, A., Johansen, A. M., Landing, W. M., Mao, J. Q., Myriokefalitakis, S., Ohnemus, D., Pasquier, B., and Ye, Y.: Perspective on identifying and characterizing the processes controlling iron speciation and residence time at the atmosphere-ocean interface, Mar. Chem., 217, 103704, 2019.

Moore, C. M., Mills, M. M., Achterberg, E. P., Geider, R. J., LaRoche, J., Lucas, M. I., McDonagh, E. L., Pan, X., Poulton, A. J., Rijkenberg, M. J. A., Suggett, D. J., Ussher, S. J., and Woodward, E. M. S.: Large-scale distribution of Atlantic nitrogen fixation controlled by iron availability, Nat. Geosci., 2, 867–871, 2009.

Myriokefalitakis, S., Ito, A., Kanakidou, M., Nenes, A., Krol, M. C., Mahowald, N. M., Scanza, R. A., Hamilton, D. S., Johnson, M. S., Meskhidze, N., Kok, J. F., Guieu, C., Baker, A. R., Jickells, T. D., Sarin, M. M., Bikkina, S., Shelley, R., Bowie, A., Perron, M. M. G., and Duce, R. A.: Reviews and syntheses: the GESAMP atmospheric iron deposition model intercomparison study, Biogeosciences, 15, 6659–6684, https://doi.org/10.5194/bg-15-6659-2018, 2018.

Myriokefalitakis, S., Tsigaridis, K., Mihalopoulos, N., Sciare, J., Nenes, A., Kawamura, K., Segers, A., and Kanakidou, M.: In-cloud oxalate formation in the global troposphere: a 3-D modeling study, Atmos. Chem. Phys., 11, 5761–5782, https://doi.org/10.5194/acp-11-5761-2011, 2011.

Oakes, M., Weber, R. J., Lai, B., Russell, A., and Ingall, E. D.: Characterization of iron speciation in urban and rural single particles using XANES spectroscopy and micro X-ray fluorescence measurements: investigating the relationship between speciation and fractional iron solubility, Atmos. Chem. Phys., 12, 745–756, https://doi.org/10.5194/acp-12-745-2012, 2012a.

Oakes, M., Ingall, E. D., Lai, B., Shafer, M. M., Hays, M. D., Liu, Z. G., Russell, A. G., and Weber, R. J.: Iron Solubility Related to Particle Sulfur Content in Source Emission and Ambient Fine Particles, Environ. Sci. Tech., 46, 6637–6644, 2012b.

Ooki, A., Nishioka, J., Ono, T., and Noriki, S.: Size dependence of iron solubility of Asian mineral dust particles, J. Geophys. Res.-Atmos, 114, D03202, https://doi.org/10.01029/02008JD010804, 2009.

Paris, R. and Desboeufs, K. V.: Effect of atmospheric organic complexation on iron-bearing dust solubility, Atmos. Chem. Phys., 13, 4895–4905, https://doi.org/10.5194/acp-13-4895-2013, 2013.

Paris, R., Desboeufs, K. V., and Journet, E.: Variability of dust iron solubility in atmospheric waters: Investigation of the role of oxalate organic complexation, Atmos. Environ., 45, 6510–6517, 2011.

Paris, R., Desboeufs, K. V., Formenti, P., Nava, S., and Chou, C.: Chemical characterisation of iron in dust and biomass burning aerosols during AMMA-SOP0/DABEX: implication for iron solubility, Atmos. Chem. Phys., 10, 4273–4282, https://doi.org/10.5194/acp-10-4273-2010, 2010.

Pye, H. O. T., Nenes, A., Alexander, B., Ault, A. P., Barth, M. C., Clegg, S. L., Collett Jr., J. L., Fahey, K. M., Hennigan, C. J., Herrmann, H., Kanakidou, M., Kelly, J. T., Ku, I.-T., McNeill, V. F., Riemer, N., Schaefer, T., Shi, G., Tilgner, A., Walker, J. T., Wang, T., Weber, R., Xing, J., Zaveri, R. A., and Zuend, A.: The acidity of atmospheric particles and clouds, Atmos. Chem. Phys., 20, 4809–4888, https://doi.org/10.5194/acp-20-4809-2020, 2020.

Sakata, K., Kurisu, M., Takeichi, Y., Sakaguchi, A., Tanimoto, H., Tamenori, Y., Matsuki, A., and Takahashi, Y.: Iron (Fe) speciation in size-fractionated aerosol particles in the Pacific Ocean: The role of organic complexation of Fe with humic-like substances in controlling Fe solubility, Atmos. Chem. Phys., 22, 9461–9482, https://doi.org/10.5194/acp-22-9461-2022, 2022.

Schroth, A. W., Crusius, J., Sholkovitz, E. R., and Bostick, B. C.: Iron solubility driven by speciation in dust sources to the ocean, Nat. Geosci., 2, 337–340, 2009.

Sedwick, P. N., Sholkovitz, E. R., and Church, T. M.: Impact of anthropogenic combustion emissions on the fractional solubility of aerosol iron: Evidence from the Sar-

gasso Sea, Geochem. Geophys. Geosyst., 8, Q10Q06, https://doi.org/10.1029/2007GC001586, 2007.

Seinfeld, J. H. and Pandis, S. N.: Atmospheric Chemistry and Physics: From Air Pollution to Climate Change (Third edition), Wiley Interscience, New York, ISBN 978-1-118-94740-1, 2016.

Shelley, R. U., Landing, W. M., Ussher, S. J., Planquette, H., and Sarthou, G.: Regional trends in the fractional solubility of Fe and other metals from North Atlantic aerosols (GEOTRACES cruises GA01 and GA03) following a two-stage leach, Biogeosciences, 15, 2271–2288, https://doi.org/10.5194/bg-15-2271-2018, 2018.

Shi, J. H., Guan, Y., Ito, A., Gao, H. W., Yao, X. H., Baker, A. R., and Zhang, D. Z.: High Production of Soluble Iron Promoted by Aerosol Acidification in Fog, Geophys. Res. Lett., 47, e2019GL086124, https://doi.org/10.1029/2019gl086124, 2020.

Shi, Z., Bonneville, S., Krom, M. D., Carslaw, K. S., Jickells, T. D., Baker, A. R., and Benning, L. G.: Iron dissolution kinetics of mineral dust at low pH during simulated atmospheric processing, Atmos. Chem. Phys., 11, 995–1007, https://doi.org/10.5194/acp-11-995-2011, 2011a.

Shi, Z. B., Woodhouse, M. T., Carslaw, K. S., Krom, M. D., Mann, G. W., Baker, A. R., Savov, I., Fones, G. R., Brooks, B., Drake, N., Jickells, T. D., and Benning, L. G.: Minor effect of physical size sorting on iron solubility of transported mineral dust, Atmos. Chem. Phys., 11, 8459–8469, https://doi.org/10.5194/acp-11-8459-2011, 2011b.

Shi, Z. B., Krom, M. D., Jickells, T. D., Bonneville, S., Carslaw, K. S., Mihalopoulos, N., Baker, A. R., and Benning, L. G.: Impacts on iron solubility in the mineral dust by processes in the source region and the atmosphere: A review, Aeolian Res., 5, 21–42, 2012.

Sholkovitz, E. R., Sedwick, P. N., and Church, T. M.: Influence of anthropogenic combustion emissions on the deposition of soluble aerosol iron to the ocean: Empirical estimates for island sites in the North Atlantic, Geochim. Cosmochim. Ac., 73, 3981–4003, 2009.

Sholkovitz, E. R., Sedwick, P. N., Church, T. M., Baker, A. R., and Powell, C. F.: Fractional solubility of aerosol iron: Synthesis of a global-scale data set, Geochim. Cosmochim. Ac, 89, 173–189, 2012.

Sun, J. X., Liu, L., Xu, L., Wang, Y. Y., Wu, Z. J., Hu, M., Shi, Z. B., Li, Y. J., Zhang, X. Y., Chen, J. M., and Li, W. J.: Key Role of Nitrate in Phase Transitions of Urban Particles: Implications of Important Reactive Surfaces for Secondary Aerosol Formation, J. Geophys. Res.-Atmos., 123, 1234–1243, 2018.

Tagliabue, A., Bowie, A. R., Boyd, P. W., Buck, K. N., Johnson, K. S., and Saito, M. A.: The integral role of iron in ocean biogeochemistry, Nature, 543, 51–59, 2017.

Tang, W., Llort, J., Weis, J., Perron, M. M. G., Basart, S., Li, Z., Sathyendranath, S., Jackson, T., Sanz Rodriguez, E., Proemse, B. C., Bowie, A. R., Schallenberg, C., Strutton, P. G., Matear, R., and Cassar, N.: Widespread phytoplankton blooms triggered by 2019–2020 Australian wildfires, Nature, 597, 370–375, 2021.

Tao, Y. and Murphy, J. G.: The Mechanisms Responsible for the Interactions among Oxalate, pH, and Fe Dissolution in $PM_{2.5}$, ACS Earth Space Chem., 3, 2259–2265, 2019.

Tao, Y., Moravek, A., Furlani, T. C., Power, C. E., VandenBoer, T. C., Chang, R. Y. W., Wiacek, A., and Young, C. J.: Acidity of Size-Resolved Sea-Salt Aerosol in a Coastal Urban Area:

Comparison of Existing and New Approaches, ACS Earth Space Chem., 6, 1239–1249, 2022.

Tian, H. Z., Wang, Y., Xue, Z. G., Cheng, K., Qu, Y. P., Chai, F. H., and Hao, J. M.: Trend and characteristics of atmospheric emissions of Hg, As, and Se from coal combustion in China, 1980–2007, Atmos. Chem. Phys., 10, 11905–11919, https://doi.org/10.5194/acp-10-11905-2010, 2010.

Wang, Y., Salana, S., Yu, H., Puthussery, J. V., and Verma, V.: On the Relative Contribution of Iron and Organic Compounds, and Their Interaction in Cellular Oxidative Potential of Ambient $PM_{2.5}$, Environ. Sci. Tech. Lett., 9, 680–686, 2022.

Wang, Y. Q., Wang, M. M., Li, S. P., Sun, H. Y., Mu, Z., Zhang, L. X., Li, Y. G., and Chen, Q. C.: Study on the oxidation potential of the water-soluble components of ambient $PM_{2.5}$ over Xi'an, China: Pollution levels, source apportionment and transport pathways, Environ. Int., 136, 105515, https://doi.org/10.1016/j.envint.2020.105515, 2020.

Wang, Z., Fu, H., Zhang, L., Song, W., and Chen, J.: Ligand-Promoted Photoreductive Dissolution of Goethite by Atmospheric Low-Molecular Dicarboxylates, J. Phys. Chem. A, 121, 1647–1656, 2017.

Wang, Z., Li, R., Cui, L., Fu, H., Lin, J., and Chen, J.: Characterization and acid-mobilization study for typical iron-bearing clay mineral, J. Environ. Sci., 71, 222–232, 2018.

Winton, V. H. L., Bowie, A. R., Edwards, R., Keywood, M., Townsend, A. T., van der Merwe, P., and Bollhofer, A.: Fractional iron solubility of atmospheric iron inputs to the Southern Ocean, Mar. Chem., 177, 20–32, 2015.

Wong, J. P. S., Yang, Y., Fang, T., Mulholland, J. A., Russell, A. G., Ebelt, S., Nenes, A., and Weber, R. J.: Fine Particle Iron in Soils and Road Dust Is Modulated by Coal-Fired Power Plant Sulfur, Environ. Sci. Technol., 54, 7088–7096, 2020.

Yang, J., Ma, L., He, X., Au, W. C., Miao, Y., Wang, W.-X., and Nah, T.: Measurement report: Abundance and fractional solubilities of aerosol metals in urban Hong Kong – insights into factors that control aerosol metal dissolution in an urban site in South China, Atmos. Chem. Phys., 23, 1403–1419, https://doi.org/10.5194/acp-23-1403-2023, 2023.

Yang, T., Chen, Y., Zhou, S., Li, H., Wang, F., and Zhu, Y.: Solubilities and deposition fluxes of atmospheric Fe and Cu over the Northwest Pacific and its marginal seas, Atmos. Environ., 239, 117763, https://doi.org/10.1016/j.atmosenv.2020.117763, 2020.

Yang, Y. and Weber, R. J.: Ultrafiltration to characterize $PM_{2.5}$ water-soluble iron and its sources in an urban environment, Atmos. Environ., 286, 119246, https://doi.org/10.1016/j.atmosenv.2022.119246, 2022.

Young, A. H., Keene, W. C., Pszenny, A. A. P., Sander, R., Thornton, J. A., Riedel, T. P., and Maben, J. R.: Phase partitioning of soluble trace gases with size-resolved aerosols in near-surface continental air over northern Colorado, USA, during winter, J. Geophys. Res.-Atmos, 118, 9414–9427, 2013.

Zhang, G. H., Lin, Q. H., Peng, L., Yang, Y. X., Jiang, F., Liu, F. X., Song, W., Chen, D. H., Cai, Z., Bi, X. H., Miller, M., Tang, M. J., Huang, W. L., Wang, X. M., Peng, P. A., and Sheng, G. Y.: Oxalate Formation Enhanced by Fe-Containing Particles and Environmental Implications, Environ. Sci. Technol., 53, 1269–1277, 2019.

Zhang, H. H., Li, R., Dong, S. W., Wang, F., Zhu, Y. J., Meng, H., Huang, C. P., Ren, Y., Wang, X. F., Hu, X. D., Li, T. T., Peng, C., Zhang, G. H., Xue, L. K., Wang, X. M., and Tang, M. J.: Abundance and Fractional Solubility of Aerosol Iron During Winter at a Coastal City in Northern China: Similarities and Contrasts Between Fine and Coarse Particles, J. Geophys. Res.-Atmos, 127, e2021JD036070, https://doi.org/10.1029/2021JD036070, 2022.

Zhang, R., Cao, J. J., Tang, Y. R., Arimoto, R., Shen, Z. X., Wu, F., Han, Y. M., Wang, G. H., Zhang, J. Q., and Li, G. H.: Elemental profiles and signatures of fugitive dusts from Chinese deserts, Sci. Total Environ., 472, 1121–1129, 2014.

Zhang, Y. X., Schauer, J. J., Shafer, M. M., Hannigan, M. P., and Dutton, S. J.: Source apportionment of in vitro reactive oxygen species bioassay activity from atmospheric particulate matter, Environ. Sci. Technol., 42, 7502–7509, 2008.

Zhou, M., Zheng, G., Wang, H., Qiao, L., Zhu, S., Huang, D., An, J., Lou, S., Tao, S., Wang, Q., Yan, R., Ma, Y., Chen, C., Cheng, Y., Su, H., and Huang, C.: Long-term trends and drivers of aerosol pH in eastern China, Atmos. Chem. Phys., 22, 13833–13844, https://doi.org/10.5194/acp-22-13833-2022, 2022.

Zhu, Y. H., Li, W. J., Lin, Q. H., Yuan, Q., Liu, L., Zhang, J., Zhang, Y. X., Shao, L. Y., Niu, H. Y., Yang, S. S., and Shi, Z. B.: Iron solubility in fine particles associated with secondary acidic aerosols in east China, Environ. Pollut., 264, 114769, https://doi.org/10.1016/j.envpol.2020.114769, 2020.

Zhu, Y., Li, W., Wang, Y., Zhang, J., Liu, L., Xu, L., Xu, J., Shi, J., Shao, L., Fu, P., Zhang, D., and Shi, Z.: Sources and processes of iron aerosols in a megacity in Eastern China, Atmos. Chem. Phys., 22, 2191–2202, https://doi.org/10.5194/acp-22-2191-2022, 2022.